

12 Dec 2015

## Evolution of Non-Metallic Inclusions in Foundry Steel Casting Processes

Marc Harris

Von Richards

*Missouri University of Science and Technology, vonlr@mst.edu*

Ronald J. O'Malley

*Missouri University of Science and Technology, omalleyr@mst.edu*

Semen Naumovich Lekakh

*Missouri University of Science and Technology, lekakhs@mst.edu*

Follow this and additional works at: [https://scholarsmine.mst.edu/matsci\\_eng\\_facwork](https://scholarsmine.mst.edu/matsci_eng_facwork)



Part of the [Metallurgy Commons](#), and the [Structural Materials Commons](#)

---

### Recommended Citation

M. Harris et al., "Evolution of Non-Metallic Inclusions in Foundry Steel Casting Processes," *Proceedings of the 69th Annual Technical and Operating Conference, Steel Founders' Society of America (SFSA) (2015, Chicago, IL)*, Steel Founders' Society of America (SFSA), Dec 2015.

This Article - Conference proceedings is brought to you for free and open access by Scholars' Mine. It has been accepted for inclusion in Materials Science and Engineering Faculty Research & Creative Works by an authorized administrator of Scholars' Mine. This work is protected by U. S. Copyright Law. Unauthorized use including reproduction for redistribution requires the permission of the copyright holder. For more information, please contact [scholarsmine@mst.edu](mailto:scholarsmine@mst.edu).

# **Kent D. Peaslee Steel Manufacturing Research Center**



Missouri University of Science & Technology

## **Evolution of Non-Metallic Inclusions in Foundry Steel Casting Processes**

Marc Harris  
Dr. Von L. Richards  
Dr. Ron O'Malley  
Dr. Simon Lekakh

# Evolution of Non-Metallic Inclusions in Foundry Steel Casting Processes

Missouri University of Science & Technology

Marc Harris  
Dr. Von L. Richards  
Dr. Ron O'Malley  
Dr. Simon Lekakh

## Abstract

The evolution of nonmetallic inclusions was examined for 4320 steel at an industrial steel foundry. The steel was followed from electric arc furnace melting through ladle refining to final casting. Timed sampling was performed at all stages of the process. Samples were analyzed using an automated SEM/EDS system. The overall evolution of oxide inclusions in terms of nucleation, growth, and flotation during liquid processing was studied using area fraction and average diameter. Chemical composition evolution was observed using a joint ternary plotting tool developed under this program. It was found that the use of zirconium as an addition for nitrogen/oxygen removal leads to a large number of  $ZrO_2$  inclusions, which is related to insufficient flotation due to the higher density of zirconia and in turn less effective calcium treatment. In addition, no  $ZrN$  formation was observed, likely due to the high FeO acid slag practice used. Argon stirring was found to reduce the flotation problems associated with the zirconium addition somewhat and significantly contribute to the removal of large size ( $>5\mu m$ ) inclusions.

## Introduction

Steel cleanliness is of increasing interest as demand increases for high quality, clean steel castings. Mechanical properties are affected by inclusion size, number, and morphology. Therefore research is being conducted to improve inclusion control thus minimizing the detrimental effects of inclusions on final properties. The evolution of nonmetallic inclusions throughout the production process must first be understood and controlled in order to control the final inclusion population.

Nonmetallic inclusions can be formed in the melt and upon solidification (indigenous) by exceeding the solubility limits of inclusion forming reactants in the liquid or can be introduced by external contamination events (exogenous). The most common source of nonmetallic inclusions is from melt reactions with dissolved oxygen. Typically, for steel castings, porosity is considered highly detrimental and the most common method to eliminate gas (CO) porosity is the use of deoxidizers (usually aluminum or silicon). This is an effective method of deoxidation, but it results in the generation of a large oxide inclusion population. These oxides can be highly problematic for certain steel grades where there are stringent specifications, having negative effects on castability, mechanical properties, and compliance with cleanliness requirements[1-8].

Current theories about the evolution of nonmetallic inclusions normally include the following stages: (i) nucleation, (ii) growth/agglomeration, and (iii) flotation[1-2]. A review of state-of-the-art theories of liquid steel refining in large scale metallurgical ladles was recently published by Zhang and Thomas[1]. Inclusion nucleation requires chemical supersaturation which is affected by the chemical affinity of active elements to

non-metal impurities (S, O, N) in solution in the melt, as well as alloy composition, temperature, and other factors[1]. Nucleation is largely understood based on surface energy minimization such that above some critical radius, a stable nucleus is successfully formed and subsequently grows. This growth will spontaneously occur when the critical radii of the nuclei are exceeded. Inclusion nucleation requires chemical supersaturation which is affected by alloy composition, additions, temperature, and other factors[1].

After nucleation, growth of a nonmetallic inclusion occurs through a variety of mechanisms, with the key phenomenon being Ostwald ripening driven by diffusion of elements and local thermodynamics. Growth by agglomeration has also been considered. For sub-micron particles the contacting mechanism for agglomeration is currently thought to be the result of Brownian collision. Somewhat larger particles however, are more affected by melt flow such as turbulent collision or differential flotation velocities according to Stoke's Law[1-2]. This agglomeration process, in the case of  $Al_2O_3$ , is more efficient when the inclusions are in the liquid state which is one goal of CaSi modification treatments. The calcium in this case leads to the formation of a  $CaO \cdot Al_2O_3$  liquid state inclusion that is both spherical and has increased tendency to agglomerate, increasing flotation velocity[1-4].

Flotation is best described by Stokes' Law for unstirred systems where the velocity of a particle is dependent on the density differential and its size according to Equation 1:

$$v_s = \frac{2(\rho_p - \rho_f)}{9\mu} gR^2 \quad (1)$$

where:  $v_s$  is the particle velocity,  $\rho_p$  is the particle density,  $\rho_f$  is the fluid density,  $g$  is the gravitational constant, and  $R$  is the particle radius. Stirring with argon gas is used to aid in inclusion flotation in the ladle. The gas enters through an eccentrically located porous plug in the ladle bottom. The stirring results in reduced content of large sized inclusions. The stirring increases net flotation by both increasing overall fluid velocity, and through inclusion wetting and attachment to the bubble itself, which typically results in reduced content of large sized inclusions[9].

The theories discussed here are well known and supported through countless experiments, but all three basic phenomena (nucleation-growth-flotation) occur simultaneously in liquid steel processing which complicates the study of nonmetallic inclusions[1-2]. It is important to consider that these mechanisms are interrelated and occurring the entire time the steel is in the liquid state. As time progresses the nucleated inclusion populations in the melt are expected to grow in size according to the prevailing growth mechanism, and enlarged particles have increased flotation velocity. Understanding the overall evolution of inclusions throughout liquid steel refining processes is critical in order to control final product cleanliness[6-7]. Recently, work has been done on the evolution of inclusions in continuous casting steelmaking processes applying an automated SEM-EDS system. This method allows for one to obtain important compositional data with statistical significance when examining such large volumes of production[10-18]. The formation of inclusions in a steel mill can be more controlled with limited oxygen exposure, narrow ranges of alloying, and consistent product geometry and size. These restrictions are often infeasible for foundries where castings are complex and variable. Work by Singh et al. examined four foundry processes using an automated SEM-EDS system and reviewed the effectiveness of calcium treatments on the inclusion population as well as discussing optimum treatments[13]. In the present study, a similar approach is used to both evaluate the deoxidation practice, the calcium treatment effectiveness

in relation to the deoxidation practice, the effect of argon stirring, and to understand the overall evolution of inclusions in the steel foundry processing route for carbon and low alloy steel castings.

## Experimental

### Industrial Process Sampling

A comprehensive study of steel melt processing at an industrial foundry was performed for three heats (melt through casting). Sampling points for the foundry can be seen in Figure 1 along with an outline of the processing steps at each sampling point, a schematic overview of the process including ladle design, as well as the time at which the samples were taken. The three heats which were sampled include: an aluminum/zirconium deoxidized heat (Heat AA), an aluminum deoxidized heat (Heat B), and an aluminum/zirconium deoxidized heat that employed argon stirring (Heat C). Heats AA and B were not argon stirred. The foundry melts were produced in a 5 ton EAF and poured using a stopper rod bottom-pour ladle. The steel was deoxidized with aluminum or aluminum and zirconium and a calcium treatment was performed using wire injection with steel jacketed CaSi wire. The calcium levels obtained in each heat after the CaSi wire treatment is given in Table 1. The reported final chemistries (via arc spectroscopy) for each heat can is presented in Table 2.

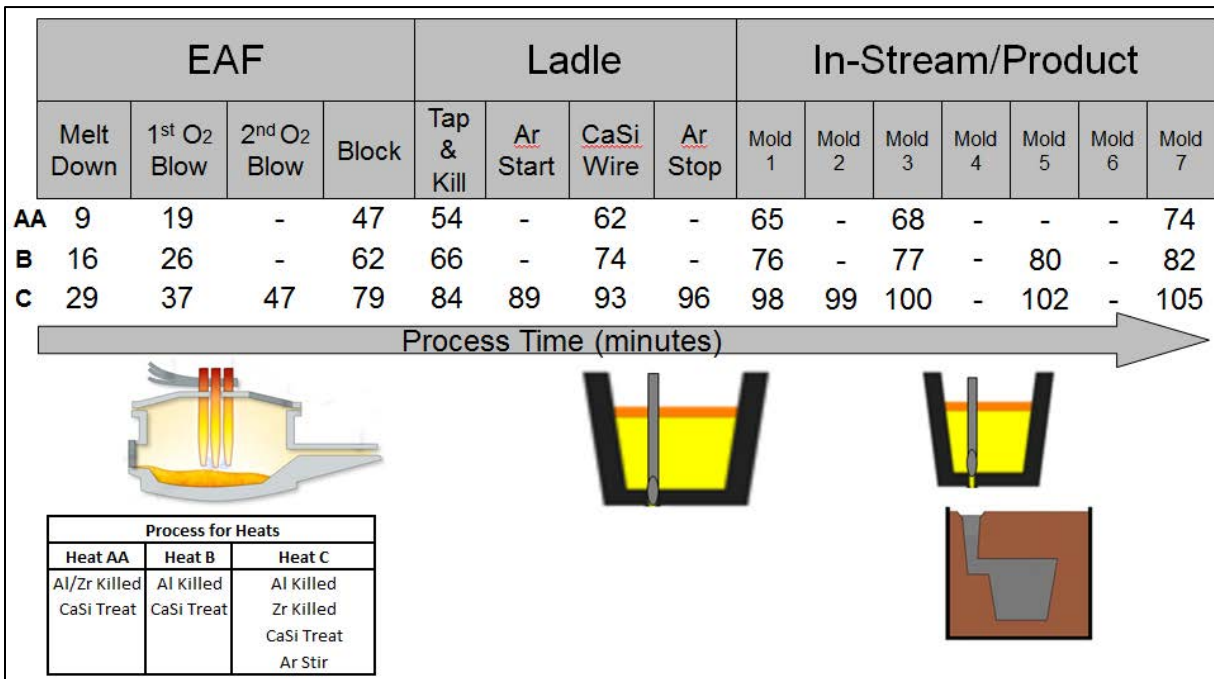


**Figure 1.** Schematic of three sampled heats (designated AA, B, and C) with process variations and sample locations shown.

**Table 1.** Calcium content (wt%) after CaSi wire injection.

	Ca (wt%)
Heat AA	0.019
Heat B	0.025
Heat C	0.024

**Table 2.** Steel chemistry (wt %) measured via arc spectroscopy.

C	Si	Mn	P	Cr	Mo	Ni	Al	Co	Cu	V	Fe
0.25 ± .043	0.52 ± .011	0.80 ± .028	0.025 ± .00005	0.76 ± .040	0.37 ± .011	1.11 ± .037	0.064 ±.013	0.013 ± .00055	0.093 ± .011	0.055 ± .008	bal.

Samples taken in the EAF and ladle prior to casting were unkilld steel chilled immersion samples taken from the top of the melt. The in-stream specimens were acquired from the liquid stream during the casting process (bottom of the ladle). The shape and sectioning method of the samples can be seen in Figure 2. The center sectioning method was used in order to minimize contamination effects, such as scale or slag entrainment that can occur at the surface. Specimens were ground using SiC media (180, 400, 600, 1200 grits), polished using 3µm diamond paste, and finished using a 0.1µm diamond paste. Metallographic preparation was done in accordance to ASTM E3-11 for all samples.

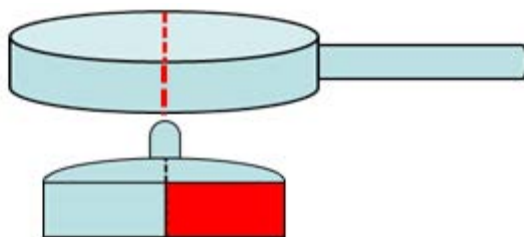


**Figure 2.** Sample sectioning method used for automated SEM/EDS scans.

### *Inclusion Analysis*

After preparation, samples were scanned using an automated ASPEX SEM/EDS system. Scans were performed using a 0.5µm minimum inclusion diameter threshold (limit of instrument), medium scan speed, 20 keV accelerating voltage, and a nominal EDS detection time of 1 second (Table 3). The step size of the search grid was 0.16µm which allows 100% detection of inclusions as small as 0.5µm in diameter[19]. Porosity was excluded from consideration using an EDS minimum count threshold of 1000, an example of which is shown in Figure 3 where a large region of porosity has been excluded from the analysis due to low counts.

**Table 3.** ASPEX SEM/EDS settings used in the analysis.

Accelerating Voltage	Emission Current	Nominal EDS Duration	Elements Considered	Exclusion Rules	Mag.	Step Size	Minimum Diameter Threshold	Max Particle Count	Reported Precision
20 keV	40-50 $\mu$ A	1 second	Mg, Al, Si, Zr, S, Ca, Ti, Mn	> 1000 counts	2000x	0.16 $\mu$ m	0.5 $\mu$ m	2500	8%

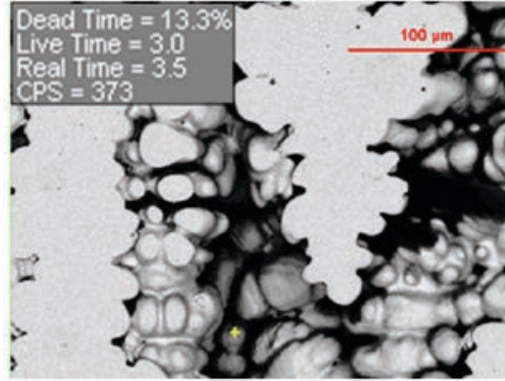


**Figure 3.** Large region of porosity with low counts per second (CPS) that leads to exclusion from analysis.

Automated analysis provides an averaged EDS spectrum near the inclusion center. In the case of complex or agglomerated inclusion types an additional post-processing filter was applied. The goal of this filtering was de-selection of sulfides from oxides through applying a sulfur concentration threshold (greater than 30% S). The statistical basis of this procedure is given in Harris et al[19]. This technique allows the monitoring of  $Al_2O_3$  modification as well as general oxide modification.

A method of calculating a mass balance from SEM-EDS data was used that allows the study of elemental content contained within inclusions. The areal average elemental composition of inclusions is calculated for each element as follows:

$$\%m = \frac{\sum(\%x)(A_{inclusion})}{A_{total}} \quad (2)$$

where:  $\%m$  is the areal average mass percent of a given element,  $\%x$  is the amount of respective element in an individual inclusion,  $A_{inclusion}$  and  $A_{total}$  are the area of the individual inclusion and total area of all measured inclusions. The mass balance calculation was performed using the compositional data obtained from the SEM-EDS inclusion analysis and Equation 3:

$$M_{ppm} = \frac{\%m A_f \rho_i w_i}{100 \rho_m} \quad (3)$$

where:  $M_{ppm}$  is the mass fraction in ppm of a given element in a sample contained within inclusions,  $\%m$  is the areal average mass percent of a given element,  $A_f$  is the total inclusion area fraction,  $\rho_i$  and  $\rho_m$  are the density of the inclusion associated with the given element and the density of the matrix respectively (taken to be iron), and  $w_i$  is the mass fraction of the given element in the associated inclusion compound.

## Results

The oxide area fraction was examined closely for Heat AA, Heat B, and Heat C and is summarized in Figure 4. The behavior of three size classes of inclusions is shown for each liquid processing stage where these heats were compared for the purpose of determining the effectiveness of argon stirring practice and zirconium additions as a nitrogen/oxygen gettinger treatment. A cut-off of 5 micron was somewhat arbitrarily used for the “large” size fraction since the 5 micron and above inclusions seemed to behave differently in terms of floatation in this industrial process. It was observed that with the addition of zirconium, the total oxide area fraction of inclusions grows with time in the ladle and that, concurrently, the inclusion size distribution shifts to larger diameters. The opposite is true when only aluminum is used. In this case, the inclusion population shifts from large area fraction with coarse particles to a finer size distribution and a lower area fraction with time in the ladle.

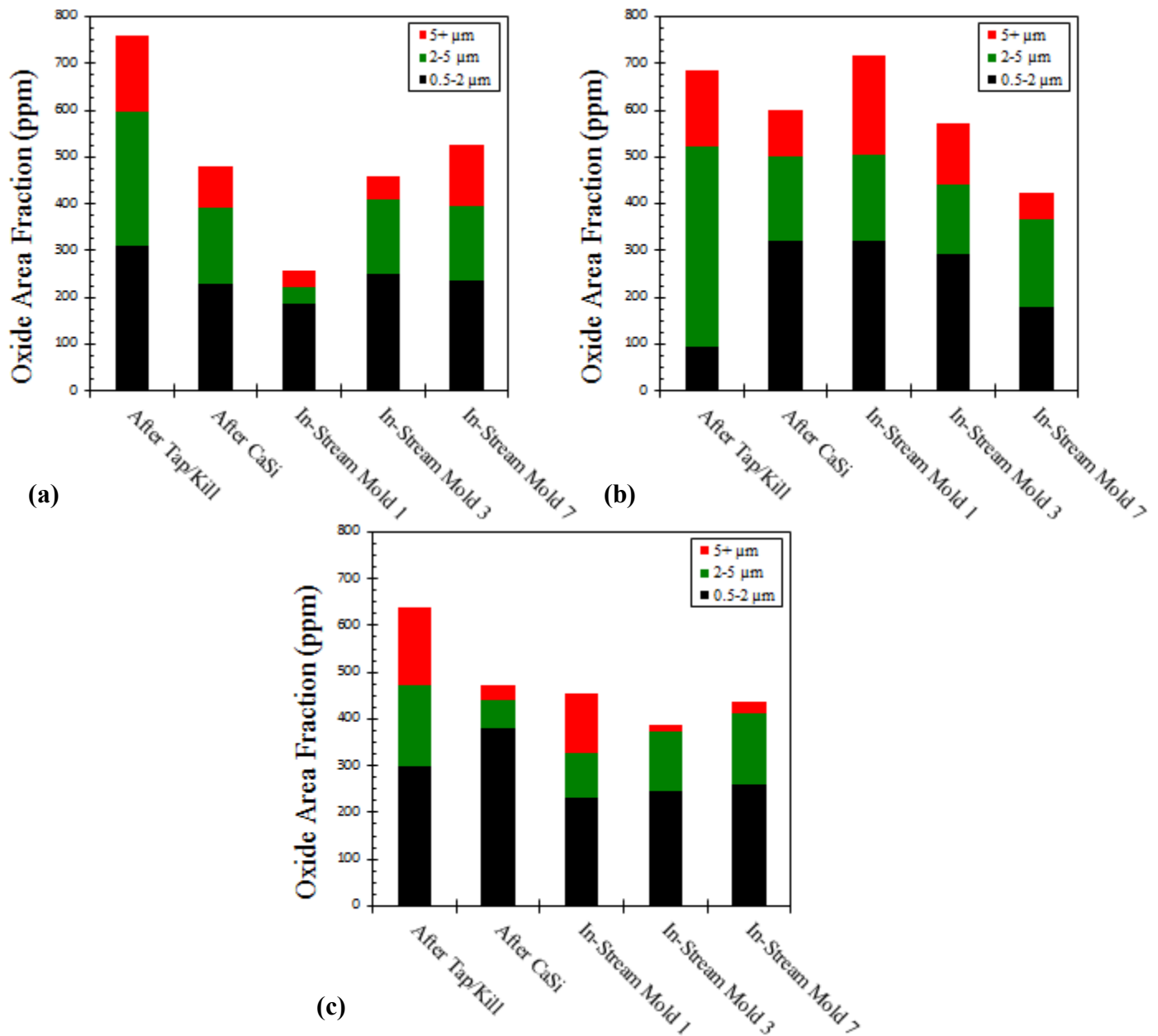


**Figure 4.** Oxide area fraction for three size ranges across a) Heat AA, b) Heat B, and c) Heat C.

The difference in behavior of the inclusion population with time in Heat AA and Heat B (Figure 5) appears to result from the difference in deoxidation practice used and its effect on inclusion flotation. Each melt was poured into 7 molds of known weight while in-stream sampling was performed from the pouring stream below the bottom of the ladle. Different molds in the sequence represent different melt levels in the ladle, where the first mold is from the bottom region of the ladle, and the last mold is near the top region. In Heat B (Al killed), the oxide area fraction was found to decrease going from the bottom of the ladle to the top over a time interval of eight minutes. In the case of Heat AA (Al+Zr killed), the opposite was found to be true: the oxide area fraction increased going from the bottom of the melt to the top. The upper quarter of the ladle appeared to accumulate an increased area fraction of inclusions compared to the bottom quarter of the ladle (450 ppm compared to 250 ppm) over a time interval of twelve minutes. By comparison, Heat B showed a drop from 700 ppm to 400 ppm oxide area fraction. Heat C, which was argon stirred, retained a uniform low level of oxide area fraction (400-450 ppm) throughout the ladle.

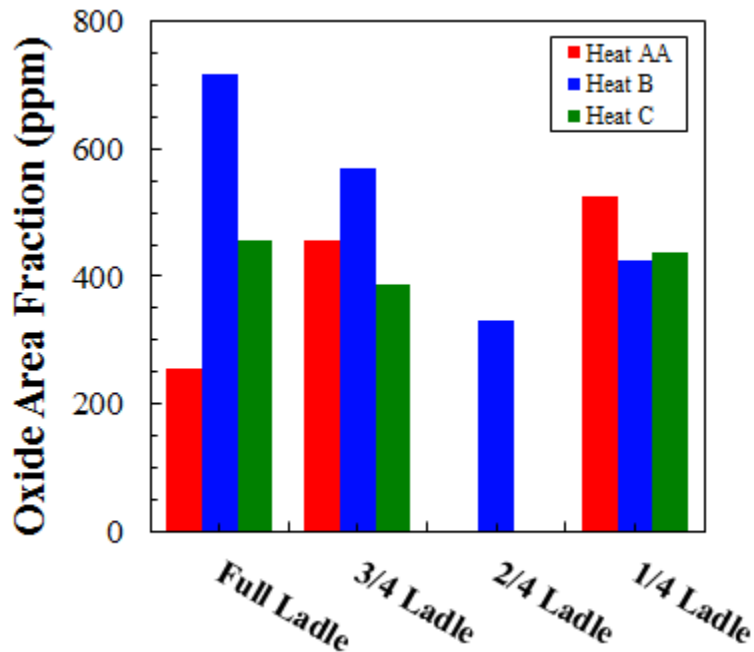
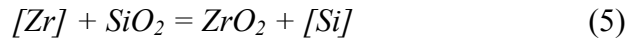
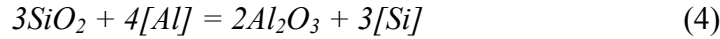


**Figure 5.** Oxide area fraction as a function of melt level for each heat.

In order to better understand the difference in treatment practice a mass balance calculation based on Eq. 2 was performed for four elements: aluminum, silicon, zirconium, and calcium (Figure 6). It was also found that the content (mass ppm) of aluminum in the samples in the form of inclusions increased immediately after deoxidation in all heats before decreasing as a result of inclusion removal. The content of silicon in inclusions decreased after deoxidation indicating that the population of silicates was reduced by the more thermodynamically stable  $\text{Al}_2\text{O}_3$  and/or  $\text{ZrO}_2$  according to Eq. 4 and Eq. 5:



The mass of zirconium reacted to form inclusions increased only after deoxidation in Heat AA and Heat C where zirconium was actually added.

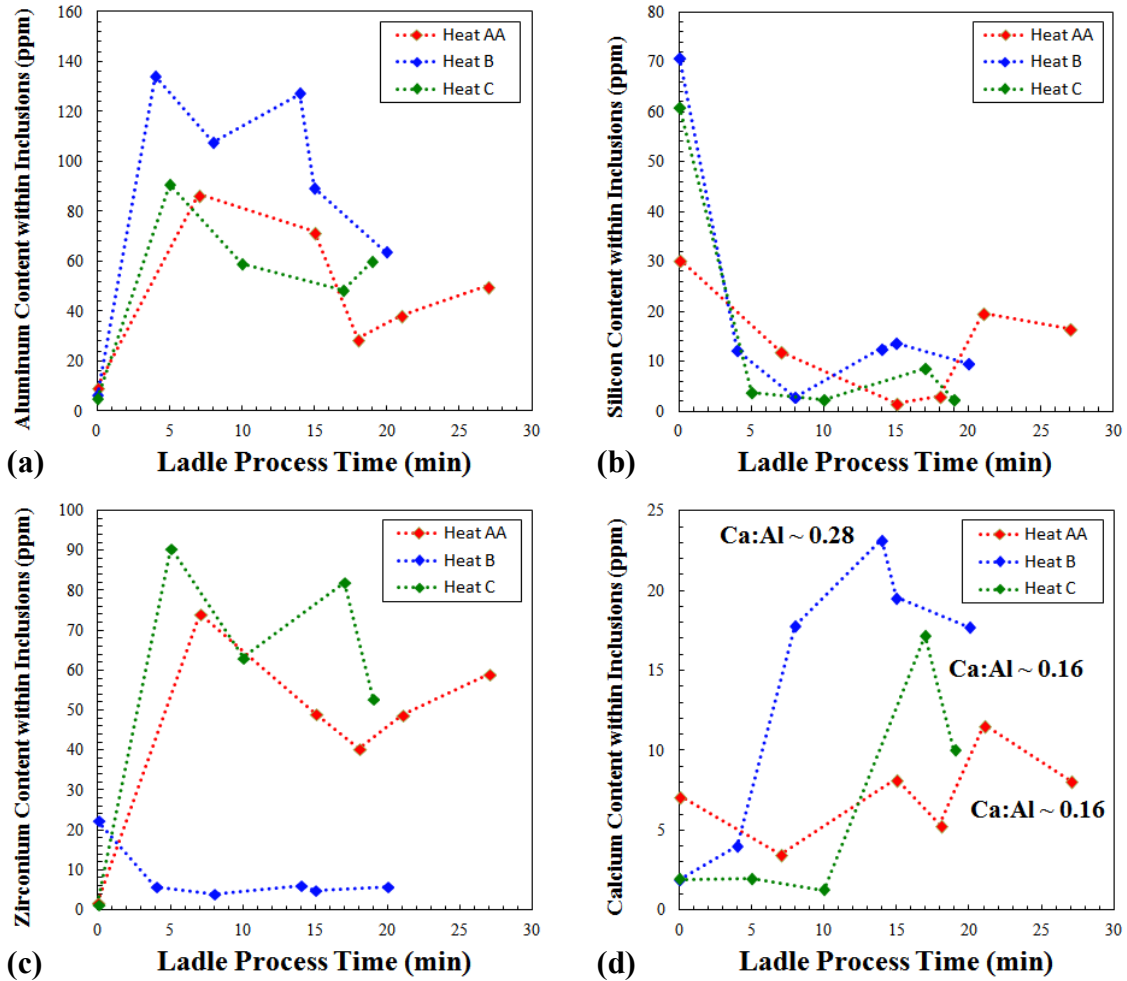
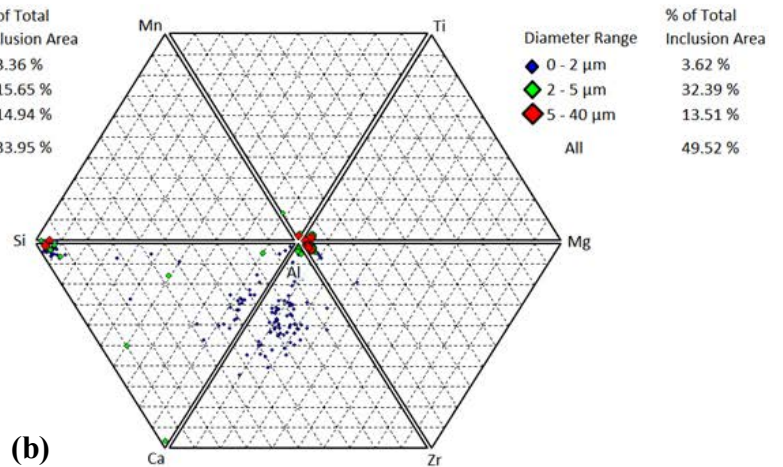
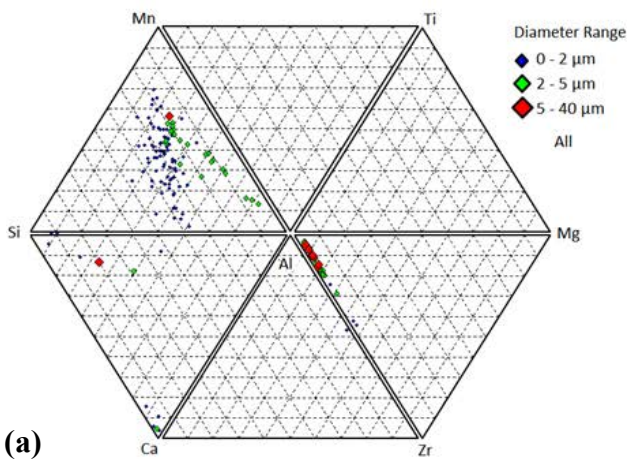


**Figure 6.** Changing total concentration of active elements within inclusions during ladle processing of analyzed heats: a) Al, b) Si, c) Zr, and d) Ca.

Calcium levels for each heat after CaSi treatment are presented in Table 1. The calcium content of inclusions increased in all heats after the treatment. However, Heat AA retained a lower mass ppm of calcium in the modified inclusions and had a lower final calcium to aluminum ratio (approx. 0.16) than that of Heat B (approx. 0.28). The slag compositions for each sampling are presented in Table 4 and an overview of the composition of the inclusion population (Figure 7) shows the progression of the inclusions for the different deoxidation practices. The composition of the oxide inclusion population after calcium addition for Heat AA can be seen to include a large number of  $ZrO_2$  rich inclusions containing some calcium. In Heat B, very little  $ZrO_2$  is present and most of the population is close to the liquid phase field of the  $CaO \cdot Al_2O_3$  binary system.

**Table 4.** Slag chemistries in wt. % of all heats at various liquid process stages.

			%SiO <sub>2</sub>	%CaO	%MgO	%Al <sub>2</sub> O <sub>3</sub>	%TiO <sub>2</sub>	%Fe <sub>2</sub> O <sub>3</sub>	%MnO <sub>2</sub>	%ZrO <sub>2</sub>	%C
Heat AA	EAF	After Melt Down	50.29	2.91	0.19	8.89	0.39	8.40	29.67	0.82	0.03
		After 1st O2 Blow	50.11	2.14	0.14	7.31	0.34	10.71	28.69	0.60	0.06
		After Block	48.83	2.03	0.16	6.93	0.33	9.30	33.31	0.53	0.17
	Ladle	After Tap/Kill	52.04	1.86	0.18	8.16	0.33	6.81	31.13	0.69	0.00
		After CaSi	49.25	2.13	0.18	9.28	0.36	6.66	32.71	0.86	0.02
Heat B	EAF	After Melt Down	51.72	2.20	0.26	6.27	0.31	18.21	20.13	0.21	0.06
		After Block	52.91	1.43	0.15	5.85	0.34	11.30	28.38	0.16	0.00
	Ladle	After Tap/Kill	51.80	1.41	0.18	8.01	0.34	8.45	30.50	0.18	0.05
		After CaSi	51.48	1.71	0.17	8.92	0.35	7.78	30.47	0.20	0.02
Heat C	EAF	After Melt Down	58.67	3.68	0.17	4.59	0.34	10.67	21.34	0.12	0.03
		After 1st O2 Blow	54.98	3.16	0.21	4.82	0.35	11.73	24.39	0.11	0.03
		After 2nd O2 Blow	54.42	2.69	0.16	4.79	0.33	13.42	23.04	0.11	0.04
		After Block	55.04	2.15	0.18	5.26	0.36	12.34	24.72	0.09	0.03
	Ladle	After Tap/Kill	52.69	2.05	0.19	8.21	0.36	8.73	28.69	0.26	0.06
		After CaSi	52.05	2.34	0.18	8.71	0.38	7.74	28.93	0.61	0.00
		After Ar Stop	52.08	2.30	0.18	8.92	0.38	7.58	29.11	0.59	0.04



(d)

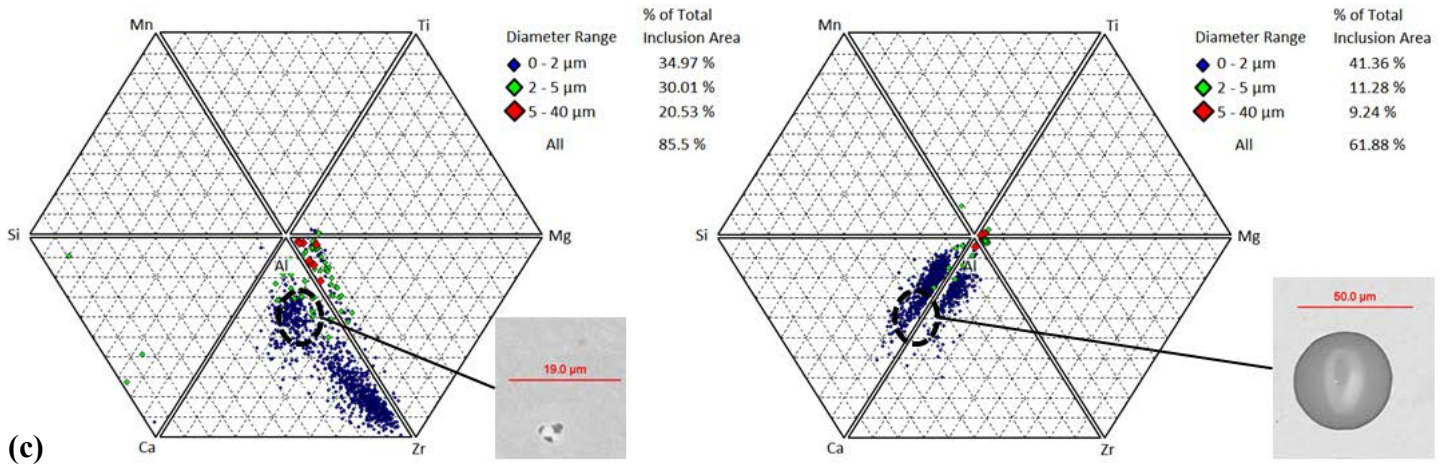


**Figure 7.** Joint ternary diagrams for a) Heat AA after deoxidation, b) Heat B after deoxidation, c) Heat AA after calcium treatment, d) Heat B after calcium treatment.

### Discussion

Measurements of total oxygen obtained by the inert gas fusion method were compared to calculated mass ppm of oxygen in the oxide inclusions that was obtained from SEM/EDS data. A linear relationship was found (Figure 8), which suggests that most of the oxygen in the steel is present in the form of oxide inclusions. Figure 9, where  $t=0$  is directly after melt down, shows that total oxygen decreases with time after the completion of oxygen blowing in the melt. This indicates that oxygen is being removed from the system. This suggests that the inclusions are being removed by flotation[1-2].

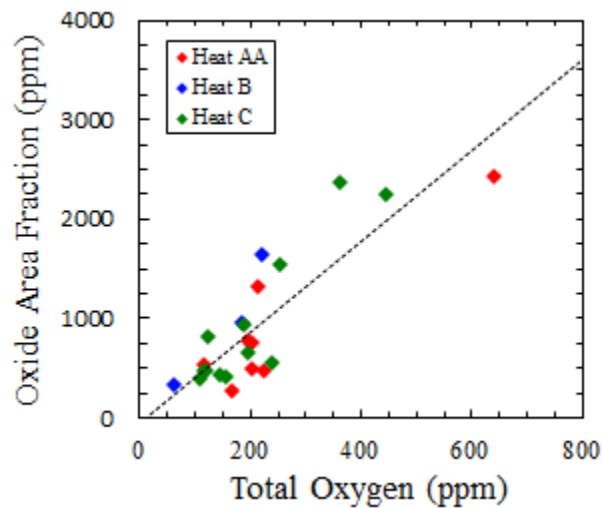


**Figure 8.** Linear relationship between oxide area fraction and total oxygen measured via inert gas fusion.

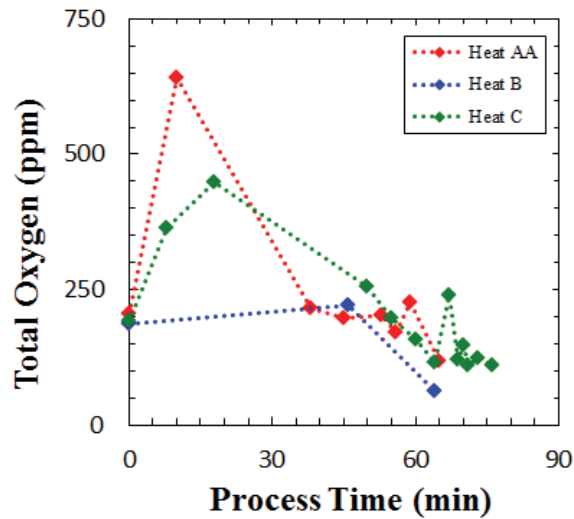


**Figure 9.** Decreasing total oxygen as a function of liquid processing time for aluminum and aluminum/zirconium treated heats.

The oxide inclusion area fraction decreased with ladle processing time after initial deoxidizing additions, which is also consistent with flotation as the mechanism for oxygen removal (Figure 10). The flotation velocity is well understood from Stoke's Law to be a function of the particle size and density. Thus inclusion growth plays a key role in the removal process. The growth of inclusions can be seen more directly by examining the average inclusion diameter in Figure 11 where the zero time is just before tapping and deoxidation. An initial decrease in size as a result of ladle deoxidation additions that nucleate large populations of small (<2  $\mu\text{m}$ ) sized inclusions occurred. A growth period follows where no ladle treatments are made and the melt is held for several minutes.

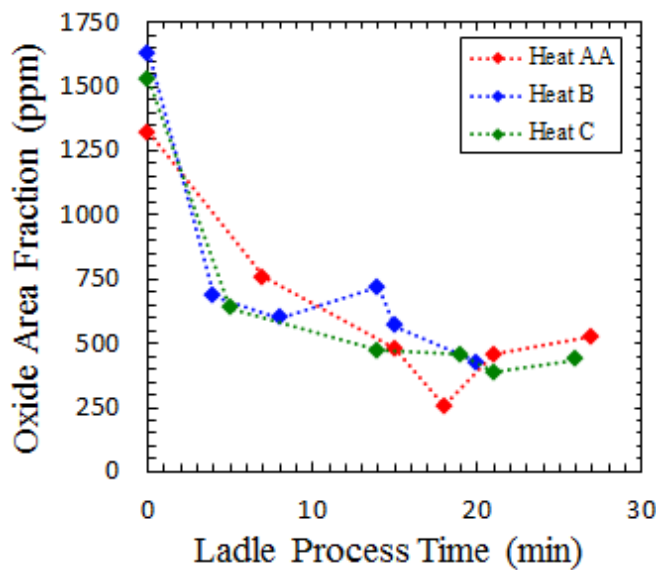


**Figure 10.** Consistent decrease observed in oxide area fraction with ladle holding time for the heats studied.

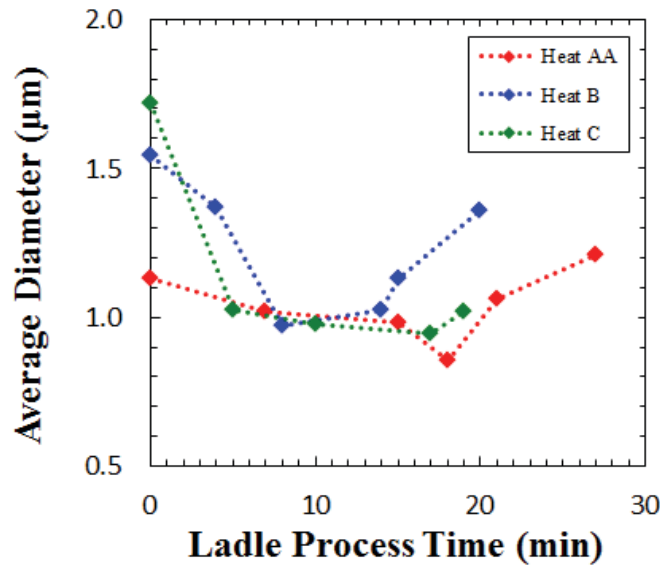


**Figure 11.** Reduction in inclusion size during deoxidation stages (nucleation) followed by a growth stage.

Deoxidation practice has a large effect on non-metallic inclusion evolution during processing. The composition change of the oxide inclusion population with time in the joint ternary plot (Figure 7) shows the effectiveness of deoxidizing method and modification clearly. The density of the type of oxide formed affects flotation. In the case of the aluminum deoxidized system,  $\text{Al}_2\text{O}_3$  was formed which has a density of approximately  $4 \text{ g/cm}^3$  while the aluminum-zirconium treated heat formed  $\text{ZrO}_2$  with a density of approximately  $5.7 \text{ g/cm}^3$ . This density difference leads to a slower flotation rate for  $\text{ZrO}_2$  rich inclusions which results in an increase in oxide area fraction at the top region of the ladle when compared to the aluminum killed heat. The  $\text{Al}_2\text{O}_3$  is more quickly removed from the system as a result of its low density and the effect of calcium treatment aimed at forming liquid  $\text{CaO} \cdot \text{Al}_2\text{O}_3$  which speeds flotation further. This faster removal rate leads to a more homogenous melt and a decrease in oxide area fraction over the time span from treatment through pouring the last production casting from the ladle. The use of argon stirring in the aluminum-zirconium treated heat (Heat C) aided the homogenization of the heat and helped mitigate the build-up of oxides in the top region of the melt by assisting inclusion flotation. It is important to note that the addition of zirconium was also expected to act as a nitrogen getter but no  $\text{ZrN}$  was observed in any samples. This may only be true because of the high oxygen potential of the 7-8%  $\text{FeO}$  and 29-32%  $\text{MnO}$  content of the ladle slag (Table 4) that was employed. The nitrogen content for Heat AA was notably high at approximately 500 ppm but still no  $\text{ZrN}$  formed (Figure 12).

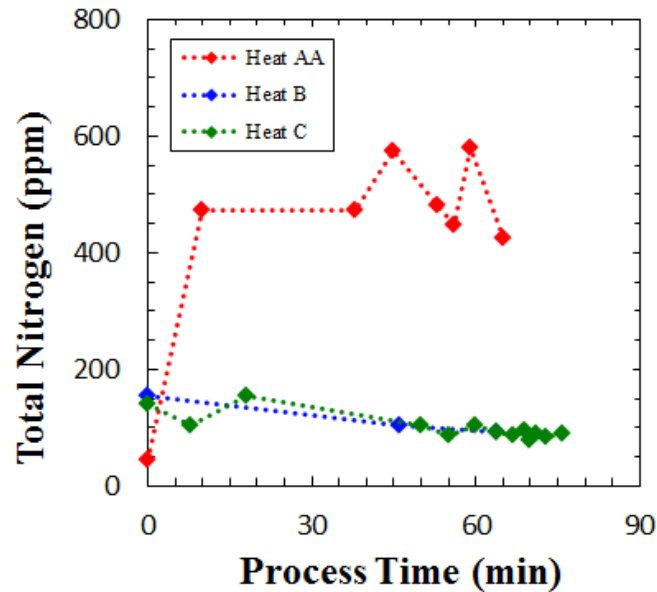


**Figure 12.** Total nitrogen content measured using inert gas fusion at each sampling point for all heats.

## Conclusions

Three industrial 4320 steel heats were followed from melting to ladle pouring in an effort to develop an understanding of the evolution of nonmetallic inclusions through a typical steel foundry process. Immersion sampling was performed at various stages during liquid steel processing in an operating industrial foundry. Three heats with different steelmaking practices were compared: (1) aluminum deoxidized, calcium treated; (2) aluminum/zirconium deoxidized, calcium treated; and (3) aluminum/zirconium deoxidized, calcium treated, argon stirred (Heats AA, B, and C respectively). In order to effectively analyze the evolution of large populations of inclusions, an automated SEM-EDS system was used which enabled a statistically significant number of nonmetallic inclusions to be analyzed.

The aluminum-zirconium treated heats had a lower calcium recovery and exhibited a slower rate of inclusion flotation because of the higher density of  $ZrO_2$  inclusions compared to the  $Al_2O_3$  inclusions generated in an aluminum killed heat. Argon stirring was found to aid in the removal of large sized ( $> 5\mu m$ ) inclusions in an aluminum-zirconium treated heat, but had little effect on the inclusion composition. It was noted that using argon stirring in conjunction with an aluminum-zirconium killing practice helped to increase the inclusion flotation rate compared to aluminum-zirconium killing without argon stirring.

## References

1. Zhang, Lifeng, and Brian Thomas. "Inclusion Nucleation, Growth, and Mixing During Steel Deoxidation." *Continuous Casting Report*: 1-19.
2. Deng, Zhiyin, and Miaoyong Zhu. "Evolution Mechanism of Non-metallic Inclusions in Al-Killed Alloyed Steel during Secondary Refining Process." *ISIJ International* 53: 450-458.
3. Higuchi, Yoshihiko, Mitsuhiro Numata, Shin Fukagawa, and Kaoru Shinme. "Inclusion Modification by Calcium Treatment." *ISIJ International* 36: 151-154.

4. Yang, Wen, Lifeng Zhang, Xinhua Wang, Ying Ren, Xuefeng Liu, and Qinglin Shan. "Characteristics of Inclusions in Low Carbon Al-Killed Steel during Ladle Furnace Refining and Calcium Treatment." *ISIJ International* 53: 1401-1410.
5. Van Ende, Marie-Aline, Muxing Guo, Joris Proost, Bart Blanpain, and Patrick Wollants. "Formation and Morphology of Al<sub>2</sub>O<sub>3</sub> Inclusions at the Onset of Liquid Fe Deoxidation by Al Addition." *ISIJ International* 51: 27-34.
6. Verma, Neerav, Petrus Pistorius, Richard Fruehan, Michael Potter, Minna Lind, and Scott Story. "Transient Inclusion Evolution During Modification of Alumina Inclusions by Calcium in Liquid Steel: Part I. Background, Experimental Techniques, and Analysis Methods." *Metallurgical and Materials Transactions B*:v42(4): 711-719.
7. Verma, N., Petrus Pistorius, Richard Fruehan, Michael Potter, Minna Lind, and Scott Story. "Transient Inclusion Evolution During Modification of Alumina Inclusions by Calcium in Liquid Steel: Part II. Results and Discussion." *Metallurgical and Materials Transactions B*: v42(4):720-729.
8. Holappa, L.. "On Physico-Chemical and Technical Limits in Clean Steel Production." *Steel Research International* 81: 869-874.
9. Lou, Wentao, and Miaoyong Zhu. "Numerical Simulations of Inclusion Behavior in Gas-Stirred Ladles." *Metallurgical and Materials Transactions B* 44B: 762-782.
10. Singh, Vintee, Kent Peaslee, and Simon Lekakh. "Use of Automated Inclusion Analysis to Evaluate the Effects of Ladle Treatment on Steel Cleanliness." *63rd SFSA T&O*.
11. Singh, Vintee, Simon Lekakh, and Kent Peaslee. "Using Automated Inclusion Analysis for Casting Process Improvements." *63rd SFSA T&O*.
12. Michelic, Susanne, Gerhard Wieser, and Christian Bernhard. "On the Representativeness of Automated SEM/EDS Analyses for Inclusion Characterisation with Special Regard to the Measured Sample Area." *ISIJ International* 51: 769-775.
13. Singh, Vintee, Simon Lekakh, Timothy Drake, and Kent Peaslee. "Process Design of Inclusion Modification in Cast Steel using Automated Inclusion Analysis." 2009. 1-11.
14. Zhang, Zhi, Anders Tilliander, Andrey Karasev, and Par Jonsson. "Simulation of the Steel Sampling Process." *ISIJ International* 50: 1746-1755.
15. Kawakami, Masahiro, Eiji Nakamura, Shuzou Matsumoto, and Seiji Yokoyama. "Morphological Classification of Inclusions in Steel by Image Processing of Micrograph." *ISIJ International* 36: 113-116.
16. Abraham, Sunday, Justin Raines, and Rick Bodnar. "Development of an Inclusion Characterization Methodology for Improving Steel Product Cleanliness." 2013. 1069-1083.
17. Kaushik, P., H. Piolet, and H. Yin. "Inclusion characterisation – tool for measurement of steel cleanliness and process control: Part 1." *Ironmaking and Steelmaking* 36: 561-571.
18. Kaushik, P., H. Piolet, and H. Yin. "Inclusion characterisation – tool for measurement of steel cleanliness and process control: Part 2." *Ironmaking and Steelmaking* 36: 572-582.
19. Harris, Marc, Obinna Adaba, Simon Lekakh, Ron O'Malley, and Von Richards. "Improved Methodology for Automated SEM/EDS Non-Metallic Inclusion Analysis of Mini-Mill and Foundry Steels." *AISTech 2015 Proceedings 2015* (2015). Print.